# Making the MOSTest of imaging genetics

*Dennis van der Meer, Ph.D.[1,2#*]; Oleksandr Frei, Ph.D.[1#]; Tobias Kaufmann, Ph.D.[1]; Alexey A. Shadrin, Ph.D.[1]; Anna Devor, Ph.D.[1,3,4]; Olav B. Smeland, M.D. Ph.D.[1]; Wes Thompson, Ph.D.[1,5]; Chun Chieh Fan, M.D. Ph.D.[5]; Dominic Holland, Ph.D.[3,5]; Lars T. Westlye, Ph.D.[1,6]; Ole A. Andreassen, M.D. Ph.D.[1] & Anders M. Dale, Ph.D.[1,5]*

1. NORMENT, Division of Mental Health and Addiction, Oslo University Hospital & Institute of Clinical Medicine, University of Oslo, Oslo, Norway
2. School of Mental Health and Neuroscience, Faculty of Health, Medicine and Life Sciences, Maastricht University, Maastricht, The Netherlands
3. Departments of Neurosciences and Radiology, University of California at San Diego, La Jolla, CA 92037, USA
4. Martinos Center for Biomedical Imaging, MGH/HMS, Charlestown, MA 02129, USA
5. Center for Multimodal Imaging and Genetics, University of California at San Diego, La Jolla, CA 92037, USA
6. Department of Psychology, University of Oslo, Oslo, Norway

*# these authors contributed equally to this work. *Corresponding author: d.v.d.meer@medisin.uio.no. Address: Kirkeveien 166, 0450 Oslo, Norway*

Keywords:
Genome-wide association study
Brain morphology
Multivariate

Word count abstract/body:
199/1598

Tables/figures/supplements:
0/4/1

Running title: Making the MOSTest of imaging genetics

A B S T R A C T

**Regional brain morphology has a complex genetic architecture, consisting of many common polymorphisms with small individual effects, which has limited the output of genome-wide association studies to date, despite its high heritability[1,2]. Given shared genetic architecture of brain regions, joint analysis of regional morphology measures in a multivariate statistical framework provides a way to enhance discovery of genetic variants with current sample sizes. While several multivariate approaches to GWAS have been put forward over the past years[3–5], none are optimally suited for complex, large-scale data. Here, we apply the Multivariate Omnibus Statistical Test (MOSTest), with an efficient computational design enabling rapid and reliable permutation-based inference, to 171 subcortical and cortical brain morphology measures from 26,502 participants of the UK Biobank (mean age 55.5 years, 52.0% female). At the conventional genome-wide significance threshold of $\alpha=5x10^{-8}$, MOSTest identifies 347 genetic loci associated with regional brain morphology, improving upon the discovery of established GWAS approaches more than threefold. Our findings implicate more than 5% of all protein-coding genes, and provide evidence for gene sets involved in neuron development and differentiation. As such, MOSTest, made publicly available, enables large steps forward in our understanding of the genetic determinants of regional brain morphology**.

Regional variations in surface area and thickness of the cerebral cortex, together with the volume of underlying subcortical structures, have been linked to much of our emotion processing and cognitive abilities, as well as the onset and course of devastating brain disorders. These brain morphological features are known to be highly heritable and to have a complex genetic architecture, involving many common genetic variants with small effect sizes[1,2].

The predominant strategy for identifying genomic loci associated with complex traits is through genome-wide association study (GWAS), a mass-univariate approach whereby the association between a single outcome measure and each of millions of genetic variants, in isolation, is tested. This is accompanied by a stringent multiple comparison correction to control the family-wise error rate, necessitating very large sample sizes to identify even relatively strong effects. To date, the largest GWAS of regional brain morphological features based on brain scans obtained from up to fifty thousand individuals, identified almost two hundred genetic variants[1], which together explained only a fraction of the reported narrow-sense heritability. These studies primarily investigate each region of interest individually, compounding the multiple comparisons correction problem.

In addition to small effect sizes, the genetic architectures of sets of regional brain features are likely to strongly overlap. Neighboring brain regions have similar functions and cytoarchitecture, indicating coordinated development[6], and thus shared genetic influences. Further, while cortical thickness and surface area have been reported to be phenotypically and genetically only weakly correlated to each other[7], many brain-related traits share a large proportion of genetic variants, even in the

absence of an overall correlation[8]. The discovery of these variants may thereby be boosted through joint analysis of these features, in a multivariate framework. This negates the application of penalties for studying multiple outcome measures, or the use of strategies that reduce phenotypic information to a single composite score, which is known to cause considerable loss of statistical power[9]. Importantly, a multivariate approach is much more consistent with the notion of the brain being an integrated unit, with highly interconnected and biologically similar brain regions, compared to univariate approaches that ignore the information shared across these component measures.

We have developed a Multivariate Omnibus Statistical Test (MOSTest), designed to boost the power of imaging genetics by capitalizing on the shared signal across related measures. MOSTest has a unique combination of computational features that sets it apart from other multivariate approaches proposed in recent years[3–5,10]; it is capable of combining large-scale genome-wide analyses of dozens of traits for tens of thousands of individuals within hours while achieving state-of-the-art statistical power. Key characteristics of MOSTest include 1) the use of Mahalanobis norm, as the sum of squared de-correlated z-values across univariate GWAS summary statistics, to integrate effects across measures into a multivariate test statistic, 2) a rapid permutation-based approach to inference, in a way that accounts for the multivariate correlation structure among phenotypes, and 3) employment of the gamma cumulative density function to fit an analytic form for the null distribution, enabling extrapolation to and beyond $5x10^{-8}$ significance. This avoids the extensive computational burden associated with a permutation-based approach which has, until now, prohibited its application in GWAS. Please see the Extended Data section for a further discussion and validation of these features.

As a comparison method, we followed an established approach recently leveraged by the Enhancing NeuroImaging Genetics through Meta-Analysis (ENIGMA) consortium[1], referred to as the min-P approach; min-P takes the smallest p-value of each SNP across the univariate GWAS, and corrects this for the effective number of traits studied[4,11], i.e. shared genetic architecture does not directly contribute to a more extreme test statistic. This method has highest power when the traits under investigation are independent from each other, as this results in higher variability of p-values and thus greater odds of a low p-value. Conversely, min-P has lowest power when traits are strongly correlated, as there is limited additional residual variance explained for the same degrees of freedom penalty[3].

Here, we applied our novel MOSTest to sets of regional brain morphology measures, to significantly improve upon previous efforts to discover the genetic loci associated with brain structure. Our sample consisted of 26,502 healthy White European participants of the UK Biobank (UKB), with a mean age of 55.5 years (standard deviation (SD) 7.4), 52.0% female. We processed T1-weighted structural MRI scans with the FreeSurfer v5.3 standard recon-all processing pipeline, producing a subset of 35 subcortical volume estimates[12], as well as subsets of surface area and cortical thickness estimates, both consisting of 68 cortical regions following the Desikan-Killiany parcellation[13], for a total set of 171 measures. All measures were pre-residualized for age, sex, scanner site, a proxy of image quality (Euler number), the first twenty genetic principal components to control for population stratification, and a global measure specific to each set of variables: mean cortical thickness for the regional thickness measures, total surface area for the area measures, and intracranial volume for the subcortical structures. Subsequently, we performed a rank-based inverse normal transformation to the residualized measures. We made use of the UKB v3 imputed data, carrying out standard quality-checks and setting a minor allele frequency threshold of .005, leaving 7.4 million SNPs. Univariate GWAS of each measure was performed with standard tools. The resulting summary statistics were then combined through MOSTest. For more details on sample composition, processing of the data, and the analysis techniques, please see the Online Methods section.

Through the multivariate GWAS, we found hundreds of independent loci surpassing the conventional whole-genome significance threshold of $\alpha=5x10^{-8}$, improving upon the discovery of all previous GWAS of brain morphology[1,2,14]. Overall, MOSTest led to a threefold higher discovery than the min-P approach, as shown in Figure 1A. The difference in performance is particularly pronounced when all features are combined, as also evident from the Miami plots shown in Figure 1B through E. This is in line with the philosophy behind MOSTest, to capitalize most on the combination of features and shared signal. As can be seen in Figure 1F, many loci identified through MOSTest were shared across the three feature subsets.

Using the MiXeR tool[8,15] we fitted a Gaussian mixture model of the null and non-null effects, and estimated for each feature set the number of SNPs involved, i.e. their polygenicity, and their effect size variance, or 'discoverability'. The results are summarized in Figure 2, depicting the estimated proportion of genetic variance explained by discovered SNPs by both approaches as a function of sample size. From the horizontal shift of the curve, we can gather that the effective sample size of MOSTest is about twice as high as min-P for most of the discovery trajectory.

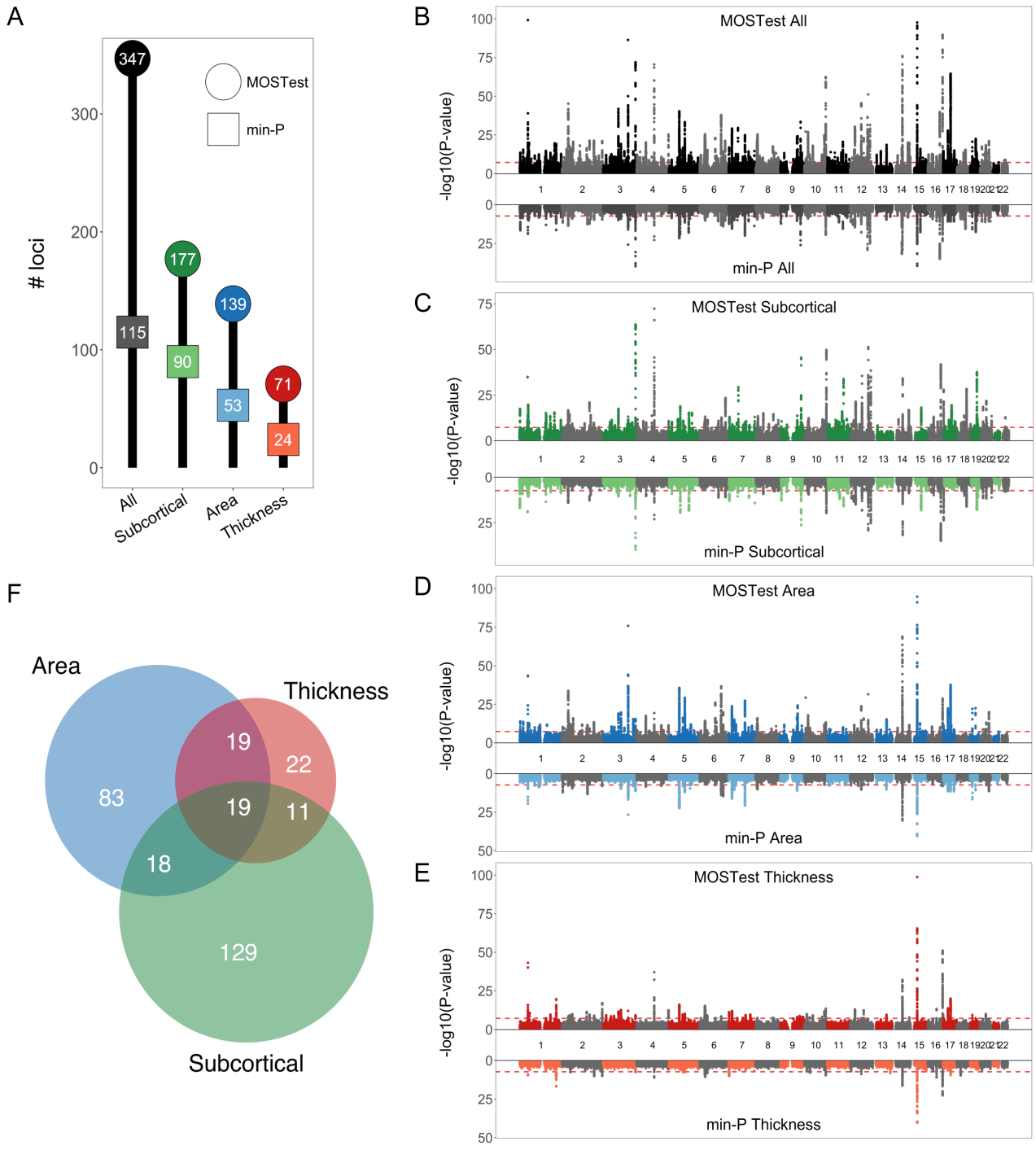


***Figure 1. Highly improved locus discovery through MOSTest. A.*** *Number of independent whole-genome significant loci identified (on the y-axis and in the bubbles) for each set of features (on the x-axis), by MOSTest (in darker colored circles) and by min-P (in lighter colored squares).* ***B - E.*** *Miami plots, contrasting the observed -log$_{10}$(p-values), shown on the y-axis, of each SNP for MOSTest (top half) with min-P (bottom half), for each of the feature sets. The x-axis shows the relative genomic location, grouped by chromosome, and the red dashed lines indicate the whole-genome significance threshold of 5x10$^{-8}$. Note, y-axis is clipped at -log$_{10}$(p-value)=100.* ***F.*** *Venn diagram depicting the number of loci, identified through MOSTest, overlapping between the three feature subsets.*

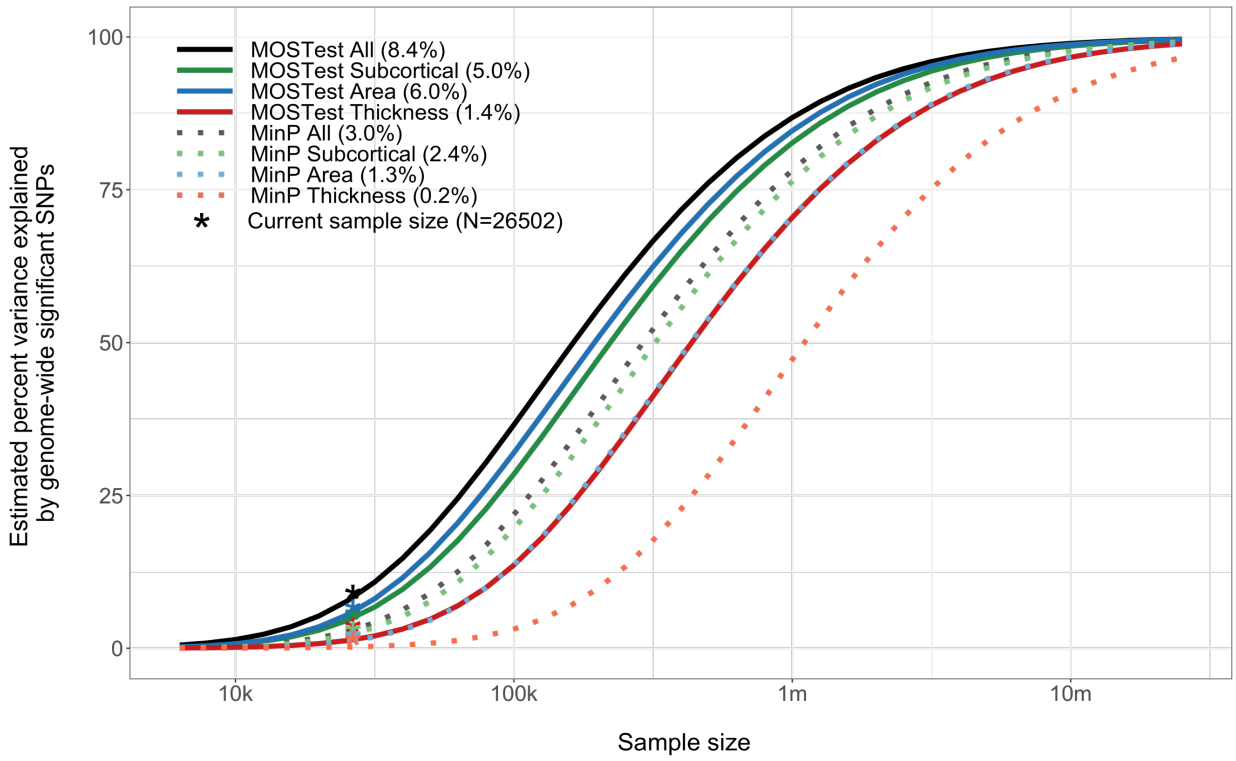


***Figure 2. MOSTest increases effective sample size.*** *Estimated percent of genetic variance explained by SNPs surpassing the genome-wide significance threshold, on the y-axis, as a function of sample size, depicted on the x-axis on a* $\log_{10}$ *scale, for each of the feature sets and for both approaches. Percentages of genetic variance explained by discovered SNPs with current sample size (N=26,502) are shown in parentheses.*

Cortical maps, depicting the morphological associations of the lead SNPs identified through MOSTest on all features with regional surface area and thickness measures, made clear that these SNPs have widespread effects, often with mixed directions, across regions and feature sets. As example, Figure 3 shows the maps for the top two hits (rs1080066 on chromosome 15, $p=1.2*10^{-305}$, and rs13107325 on chromosome 4, $p=3.1*10^{-124}$), all other maps are available in the Supplementary Material. These maps revealed anterior-posterior gradients as well as hemisphere-specific effects of some of the lead SNPs, in line with previously reported genetic patterns of the brain[16–18].

Gene-level analyses, using Multi-marker Analysis of GenoMic Annotation (MAGMA)[19,20], indicated that 1034 out of all 18,775 protein coding genes (i.e. 5.5%) were significant, with a p-value below a Bonferroni corrected threshold of $\alpha$=.05/18,775. Figure 4A shows the number of significant genes for each (sub)set of features. Through competitive gene-set analyses we identified 136 significant Gene Ontology sets for MOSTest applied to all features, the vast majority of which related to (regulation of) neuronal development and differentiation, with Figure 4B listing the top fifteen.

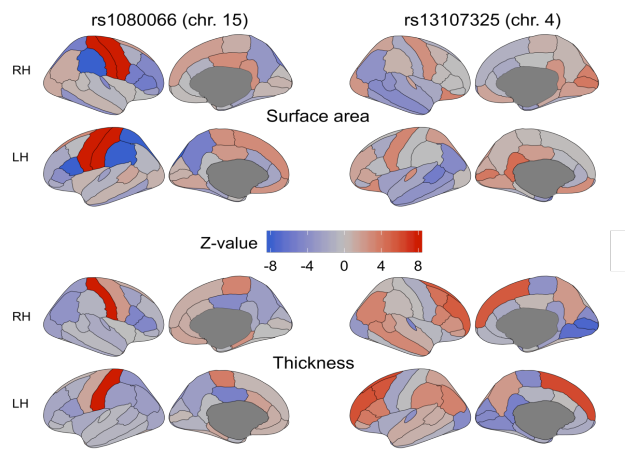


***Figure 3. The genetic variants identified through MOSTest have distributed effects across the cortex.*** *Z-values from the univariate GWAS for each cortical region for the two most significant lead SNPs from MOSTest applied to all features combined (left two columns for rs1080066 on chromosome 15, and right two columns for rs13107325 on chromosome 4). The top two rows show the effects of the SNPs on regional surface area, and the bottom two on cortical thickness. Positive effects of carrying the minor allele are shown in red, and negative in blue. Note: the absolute Z-value scaling is clipped at 8 (*$p=1.2*10^{-15}$*), RH=right hemisphere, LH=left hemisphere.*

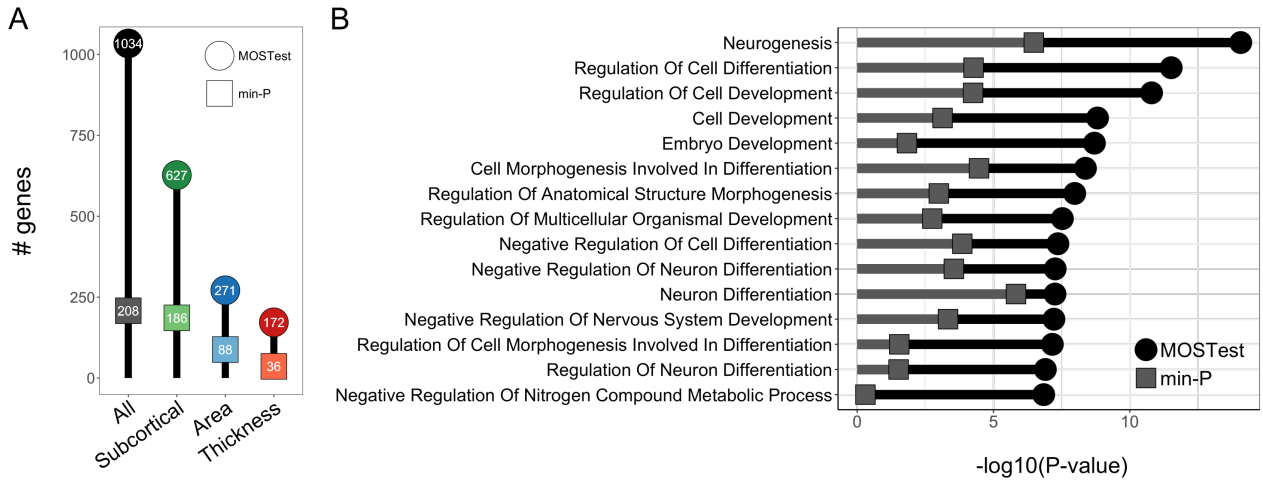


***Figure 4. Functional mapping and annotation indicates high neurobiological relevance of our findings. A.*** *Number of whole-genome significant genes identified (on the y-axis and in the bubbles) for each set of features (on the x-axis), by MOSTest (in darker colored circles) and by min-P (in lighter colored squares).* ***B.*** *Results from the gene-set analyses following the application of the multivariate GWAS on all brain features. The fifteen most significant Gene Ontology sets for MOSTest are listed on the y-axis and -log10(p-values) are shown on the x-axis. MOSTest Bonferroni corrected p-values are indicated by black circles, min-P in grey squares.*

Here, using our novel MOSTest approach to GWAS, we identified an unprecedented number of loci and genes associated with regional brain morphology. The success of this approach is indicative of the presence of extensive shared genetic architecture across brain regions and across morphological measures, attesting to the importance of estimating levels of genetic overlap beyond those indicated by simple correlations[8] and pleading for techniques that boost discovery of genetic determinants by making use of shared signal between traits[21]. Indeed, overlapping genetic determinants are to be expected given the intricacy of brain development, with myriad molecular mechanisms operating across regional borders defined by gross morphological features. This is in accordance with high levels of pleiotropy across many brain-related traits and disorders[22]. Therefore, our multivariate strategy is better tailored to the complex biological processes we aim to understand than conventional univariate approaches, as confirmed by our identification of highly significant links to gene sets of neuronal development and differentiation. We estimate that, with the large gain of power and consequently lower required sample sizes of MOSTest, we will be able to uncover the majority of SNPs determining brain morphology in the upcoming years; the UK Biobank initiative, for instance, is set to release neuroimaging data of a 100,000 individuals by 2022[23], which we predict will enable MOSTest to uncover about 40% of SNPs associated with regional brain morphology. Its output is ideally suited for secondary analyses and follow-up studies to investigate the relation between the set of loci discovered and individual features, with a much decreased multiple-comparisons burden. We have therefore made the MOSTest code publicly available, see Online Methods. As such, this approach may provide a highly fruitful strategy to uncover the genetic determinants of brain structure and function and other complex human phenotypes consisting of correlated component measures, such as mental, cognitive or cardiometabolic phenotypes, by taking advantage of the rich multivariate datasets now available.

## Author contributions

A.M.D., O.F., D.v.d.M and O.A.A. conceived the study; D.v.d.M., O.F., T.K. and A.M.D. pre-processed the data. D.v.d.M., O.F. and A.M.D. performed all analyses, with conceptual input from O.A.A.; All authors contributed to interpretation of results; D.v.d.M. drafted the manuscript and all authors contributed to and approved the final manuscript.

## Materials & Correspondence.

The data incorporated in this work were gathered from public resources. The code is available via https://github.com/precimed/mostest (GPLv3 license). Correspondence and requests for materials should be addressed to d.v.d.meer@medisin.uio.no

## References

1. Grasby, K. L. *et al.* The genetic architecture of the human cerebral cortex. *bioRxiv* 399402 (2018). doi:10.1101/399402
2. Satizabal, C. L. *et al.* Genetic Architecture of Subcortical Brain Structures in Over 40,000 Individuals Worldwide. *bioRxiv* 173831 (2017).
3. Porter, H. F. & O'Reilly, P. F. Multivariate simulation framework reveals performance of multi-trait GWAS methods. *Sci. Rep.* **7**, 38837 (2017).
4. O'Reilly, P. F. *et al.* MultiPhen: joint model of multiple phenotypes can increase discovery in GWAS. *PLoS One* **7**, e34861 (2012).
5. Ferreira, M. A. R. & Purcell, S. M. A multivariate test of association. *Bioinformatics* **25**, 132–133 (2008).
6. Alexander-Bloch, A., Giedd, J. N. & Bullmore, E. Imaging structural co-variance between human brain regions. *Nat.*

*Rev. Neurosci.* **14**, 322 (2013).
7. Panizzon, M. S. *et al.* Distinct genetic influences on cortical surface area and cortical thickness. *Cereb. Cortex* bhp026 (2009).
8. Frei, O. *et al.* Bivariate causal mixture model quantifies polygenic overlap between complex traits beyond genetic correlation. *Nat. Commun.* **10**, 2417 (2019).
9. Van Der Sluis, S., Verhage, M., Posthuma, D. & Dolan, C. V. Phenotypic complexity, measurement bias, and poor phenotypic resolution contribute to the missing heritability problem in genetic association studies. *PLoS One* **5**, e13929 (2010).
10. Wu, C. Multi-trait genome-wide analyses of the brain imaging phenotypes in UK Biobank. *bioRxiv* 758326 (2019). doi:10.1101/758326
11. Van der Sluis, S., Posthuma, D. & Dolan, C. V. TATES: efficient multivariate genotype-phenotype analysis for genome-wide association studies. *PLoS Genet.* **9**, e1003235 (2013).
12. Fischl, B. *et al.* Whole brain segmentation: automated labeling of neuroanatomical structures in the human brain. *Neuron* **33**, 341–355 (2002).
13. Desikan, R. S. *et al.* An automated labeling system for subdividing the human cerebral cortex on MRI scans into gyral based regions of interest. *Neuroimage* **31**, 968–980 (2006).
14. Elliott, L. T. *et al.* Genome-wide association studies of brain imaging phenotypes in UK Biobank. *Nature* **562**, 210 (2018).
15. Holland, D. *et al.* Beyond SNP Heritability: Polygenicity and Discoverability of Phenotypes Estimated with a Univariate Gaussian Mixture Model. *bioRxiv* 498550 (2019). doi:10.1101/498550
16. Chen, C.-H. *et al.* Hierarchical genetic organization of human cortical surface area. *Science* **335**, 1634–1636 (2012).
17. Chen, C.-H. *et al.* Genetic topography of brain morphology. *Proc. Natl. Acad. Sci.* **110**, 17089 LP – 17094 (2013).
18. Kong, X.-Z. *et al.* Mapping cortical brain asymmetry in 17,141 healthy individuals worldwide via the ENIGMA Consortium. *Proc. Natl. Acad. Sci.* **115**, E5154–E5163 (2018).
19. de Leeuw, C. A., Mooij, J. M., Heskes, T. & Posthuma, D. MAGMA: generalized gene-set analysis of GWAS data. *PLoS Comput. Biol.* **11**, e1004219 (2015).
20. Watanabe, K., Taskesen, E., Bochoven, A. & Posthuma, D. Functional mapping and annotation of genetic associations with FUMA. *Nat. Commun.* **8**, 1826 (2017).
21. Andreassen, O. A. *et al.* Improved detection of common variants associated with schizophrenia and bipolar disorder using pleiotropy-informed conditional false discovery rate. *PLoS Genet.* **9**, e1003455 (2013).
22. Watanabe, K. *et al.* A global overview of pleiotropy and genetic architecture in complex traits. *Nat. Genet.* 1–10 (2019).
23. Miller, K. L. *et al.* Multimodal population brain imaging in the UK Biobank prospective epidemiological study. *Nat. Neurosci.* **19**, 1523–1536 (2016).
24. Sudlow, C. *et al.* UK biobank: an open access resource for identifying the causes of a wide range of complex diseases of middle and old age. *PLoS Med.* **12**, e1001779 (2015).
25. Bycroft, C. *et al.* The UK Biobank resource with deep phenotyping and genomic data. *Nature* **562**, 203–209 (2018).
26. Bensimhoun, M. N-dimensional cumulative function, and other useful facts about gaussians and normal densities. *Jerusalem, Isr. Tech. Rep* 1–8 (2009).
27. Finucane, H. K. *et al.* Partitioning heritability by functional annotation using genome-wide association summary statistics. *Nat. Genet.* **47**, 1228 (2015).

**Acknowledgements**

The authors were funded by the Research Council of Norway (276082, 213837, 223273, 204966/F20, 229129, 249795/F20, 225989, 248778, 249795), the South-Eastern Norway Regional Health Authority (2013-123, 2014-097, 2015-073, 2016-064, 2017-004), Stiftelsen Kristian Gerhard Jebsen (SKGJ-Med-008), The European Research Council (ERC) under the European Union's Horizon 2020 research and innovation programme (ERC Starting Grant, Grant agreement No. 802998) and National Institutes of Health (R01MH100351, R01GM104400). This work was partly performed on the TSD (Tjeneste for Sensitive Data) facilities, owned by the University of Oslo, operated and developed by the TSD service group at the University of Oslo, IT-Department (USIT). (tsd-drift@usit.uio.no). Computations were also performed on resources provided by UNINETT Sigma2 - the National Infrastructure for High Performance Computing and Data Storage in Norway.

**Competing financial interests**.

Dr. Andreassen has received speaker's honorarium from Lundbeck, and is a consultant to HealthLytix. Dr. Dale is a Founder of and holds equity in CorTechs Labs, Inc, and serves on its Scientific Advisory Board. He is a member of the Scientific Advisory Board of Human Longevity, Inc. and receives funding through research agreements with General Electric Healthcare and Medtronic, Inc. The terms of these arrangements have been reviewed and approved by UCSD in accordance with its conflict of interest policies. The other authors declare no competing financial interests.

## Online Methods

### *Sample*

We made use of data from participants of the UKB population cohort, fetched from the data repository under accession number 27412. The composition, set-up, and data gathering protocols of the UKB have been extensively described elsewhere[24]. For this study, we selected White Europeans that had undergone the neuroimaging protocol. We excluded 1094 individuals with a primary or secondary ICD10 diagnosis of a neurological or mental disorder, as well as 594 individuals with bad structural scan quality as indicated by an age and sex-adjusted Euler number more than three standard deviations lower than the scanner site mean. Our final sample size was n=26502, with a mean age of 55.5 years (SD=7.4). 52.0% of the sample was female.

### *Data preprocessing*

T1 scans were collected from three scanning sites throughout the United Kingdom, all on identical Siemens Skyra 3T scanners with a 32-channel receive head coil. The UKB core neuroimaging team has published extensive information on the applied scanning protocols and procedures, which we refer to for more details[23]. The T1 scans were fetched from the UKB data repositories and stored locally at the secure computing cluster of the University of Oslo. We applied the standard recon-all -all processing pipeline of Freesurfer v5.3, performing automated surface-based morphometry and subcortical segmentation[12,13]. From the output, we extracted the sets of regional subcortical and cortical morphology measures, as well as estimated intracranial volume (eICV). Extended Data Table 1 contains all the regional morphology measures, per subset, included in the current study. For each of these, we included both the left and right hemisphere measure, if applicable.

We subsequently regressed out age, sex, scanner site, Euler number, and the first twenty genetic principal components from each measure. We further regressed out a global measure specific to each of the feature subsets: eICV for the subcortical volumes, mean thickness for the regional thickness measures, and total surface area for the regional surface area measures. This was done to ensure we are studying the genetic determinants of regional brain morphology rather than global effects. Following this, we applied rank-based inverse normal transformation to the residuals of each measure, leading to normally distributed input into the univariate GWAS. See the Extended Data section for a more in-depth discussion of the importance of this normalization procedure.

### *Univariate GWAS procedure*

We made use of the UKB v3 imputed data, which has undergone extensive quality control procedures as described by the UKB genetics team[25]. After converting the BGEN format to PLINK binary format, we additionally carried out standard quality check procedures, including filtering out individuals with more than 10% missingness, SNPs with more than 5% missingness, and SNPs failing the Hardy-Weinberg equilibrium test at $p=1*10^{-9}$. We further set a minor allele frequency threshold of 0.005, leaving 7,428,630 SNPs.

The univariate GWAS on each of the 171 pre-residualized and normalized regional brain morphology measures were carried out using the standard additive model of linear association between genotype vector, $g_j$, and phenotype vector, $y$. To speed up calculations we implemented the association test directly in MOSTest software. Since we are dealing with pre-residualized measures, statistical significance was assessed from Pearson's correlation coefficient $r_j = corr(y, g_{.j})$, as implemented in MATLAB's corr function. This is equivalent to testing significance of the regression slope, $\hat{\beta}_j$, as both $\hat{\beta}_j$ and $r_j$ are assumed

to be $t$-distributed and have the same $t$-value: $t_j = \beta_j / se(\beta_j) = r_j / se(r_j) = r_j \sqrt{N-2} / \sqrt{1-r_j^2}$, and therefore the same p-value, equal to Student's t cumulative distribution function (cdf) with $N-2$ degrees of freedom: $P_{val,j} = 2\, tcdf(-|t_j|, N-2)$, where N is the sample size. Further, we validated that the above procedure produces the same results as the association test implemented in the commonly used PLINK's additive model.

*The MOSTest procedure*

The MOSTest test statistic for a given SNP is calculated as Mahalanobis norm $t_{MOST} = z' \mathbf{R}^{-1} z$ from the multivariate vector of z scores, comprised of N univariate GWAS summary statistics for that SNP, where matrix **R** gives the correlation structure of z scores, estimated from the permuted data. The null hypothesis of the MOSTest is that z vector is distributed as a multivariate normal random variable with zero mean and known variance-covariance matrix, given by **R**. To compute the theoretical p-value of the MOSTest test statistic, we need to calculate the multivariate normal probability of an event that $t_{MOST} = z' \mathbf{R}^{-1} z$ exceeds a certain threshold. It is known that this probability is given by chi-square distribution with N degrees of freedom, or, equivalently, a gamma distribution, Gamma(N/2,0.5)[26]. Instead of using theoretical values, we fit the two free parameters of the Gamma(a,b) distribution to the observed distribution of $t_{MOST}$ under permutation, as this resulted in different scale parameter (b=0.434, instead of the theoretical b=0.5). The p-value of the MOSTest test statistic is then simply obtained from a cumulated distribution function of the gamma distribution, i.e. $p_{MOST}=CDF_{gamma(a,b)}(z' \mathbf{R}^{-1} z)$.

The distribution of the MOSTest test statistic under the null is estimated empirically using permutations. For each SNP, we randomly permute the genotype vector, and then calculate the association statistic $z_{perm}$ between the permuted genotype vector and each of the measures. Permutation is done in a way that preserves the multivariate correlation structure, ensuring correct p-values, even when including measures that correlate nearly perfectly with each other. Note that for a given SNP we perform just one permutation, and thus runtime of MOSTest is just twice the time of running a standard GWAS on all measures.

Controlling for covariates, such as genetic principal components, is done through pre-residualization of all input measures, i.e. we replace the measure with corresponding residual after multiple linear regression of the measure on the covariates. Additionally, we perform a rank-based inverse normal transformation of the residualized measures, to ensure that z-scores forming the input to MOSTest are normally distributed.

MOSTest code is made publicly available through GitHub, https://github.com/precimed/mostest.

*Gene-set analyses*

We made use of the Functional Mapping and Annotation of GWAS (FUMA) online platform (https://fuma.ctglab.nl/) to further process the output from MOSTest and min-P. Through FUMA, we carried out MAGMA-based gene analyses using default settings, which entail the application of a SNP-wide mean model and use of the 1000 Genomes Phase 3 EUR reference panel. Gene-set analyses were done in a similar manner, restricting the sets under investigation to those part of the Gene Ontology biological processes subset (n=4436), as listed in MsigdB v5.2.

## Extended Data

*Morphological features included*

Please see Extended Data Table 1 for an overview of all regional morphological features included in the analyses. We included all features outputted by the default Freesurfer subcortical and cortical processing streams, except for the range of global measures, CSF, surface holes, vessels, optic chiasm and hypointensities, as we did not consider these measures of regional brain morphology.

***Extended Data Table 1.*** *Regional brain morphology outcome measures, per subset, included in the study.*

| *Subcortical Volumes* | Surface Area | Thickness |
|---|---|---|
| Lateral Ventricle | Bankssts | Bankssts |
| Inferior Lateral Ventricle | Caudalanteriorcingulate | Caudalanteriorcingulate |
| Cerebellum White Matter | Caudalmiddlefrontal | Caudalmiddlefrontal |
| Cerebellum Cortex | Cuneus | Cuneus |
| Thalamus Proper | Entorhinal | Entorhinal |
| Caudate | Fusiform | Fusiform |
| Putamen | Inferiorparietal | Inferiorparietal |
| Pallidum | Inferiortemporal | Inferiortemporal |
| 3rd Ventricle* | Isthmuscingulate | Isthmuscingulate |
| 4th Ventricle* | Lateraloccipital | Lateraloccipital |
| Brain Stem | Lateralorbitofrontal | Lateralorbitofrontal |
| Hippocampus | Lingual | Lingual |
| Amygdala | Medialorbitofrontal | Medialorbitofrontal |
| Accumbens Area | Middletemporal | Middletemporal |
| Ventral Diencephalon | Parahippocampal | Parahippocampal |
| Choroid Plexus | Paracentral | Paracentral |
| 5th Ventricle* | Parsopercularis | Parsopercularis |
| CC Posterior* | Parsorbitalis | Parsorbitalis |
| CC Mid Posterior* | Parstriangularis | Parstriangularis |
| CC Central* | Pericalcarine | Pericalcarine |
| CC Mid Anterior* | Postcentral | Postcentral |
| CC Anterior* | Posteriorcingulate | Posteriorcingulate |
| | Precentral | Precentral |
| | Precuneus | Precuneus |
| | Rostralanteriorcingulate | Rostralanteriorcingulate |
| | Rostralmiddlefrontal | Rostralmiddlefrontal |
| | Superiorfrontal | Superiorfrontal |
| | Superiorparietal | Superiorparietal |
| | Superiortemporal | Superiortemporal |
| | Supramarginal | Supramarginal |
| | Frontalpole | Frontalpole |
| | Temporalpole | Temporalpole |
| | Transversetemporal | Transversetemporal |
| | Insula | Insula |

*Note: * not bilateral*

*Validation and formal comparison between MOSTest and other tools*

Current multivariate approaches, such as canonical correlation analysis as implemented in MV-PLINK[5] and ordinal regression as implemented in MultiPhen[4], perform a multiple regression in an opposite direction: the genotype vector is used as an outcome variable, while each phenotype is turned into an explanatory variable. The p-value is then calculated from an F-test, which tests for an association between the genotype vector and the most predictive linear combination of phenotypes at each SNP. Extended Data Figure 1 compares the -log10(p-value), calculated by MV-PLINK and MOSTest. MV-PLINK takes 10,000x longer to run (requiring approximately 250K CPU hours, instead of 24 CPU hours with MOSTest), it was therefore infeasible to run the analysis on the entire set of 7.4M SNPs. Instead we tested a set of 356 LD-independent SNPs (clumped at LD r2=0.6) with a p-value from min-P below the genome-wide significance threshold. The results show very high correlation (r=0.9976) between MV-PLINK and MOSTest -log10(p-values), with median of 14.16 (MOSTest) versus 14.40 (MV-PLINK).

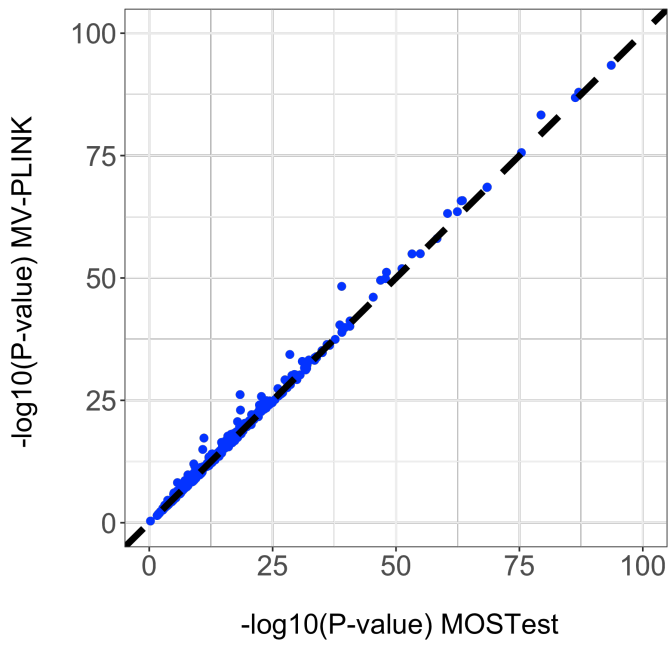


***Extended Data Figure 1.*** *Comparison between MV-PLINK and MOSTest for a selected set of 356 SNPs, showing high correlation (r=0.9976) between MV-PLINK and MOSTest -log10(p-values).*

Another recently developed multivariate test, aMAT[10], uses the same test statistic as MOSTest, but after applying regularization (spectral filtering) to the correlation matrix R. In our data regularization wasn't necessary, as the conditioning number was reasonably low, see Extended Data Table 2, leading to a well-defined matrix $R^{-1}$.

***Extended Data Table 2****. The conditioning number of the variance-covariance matrix (R), parameters of the Beta distribution (in Min-P test) and Gamma distribution (in MOSTest).*

| | #features | cond(R) | Beta_a | Beta_b | Gamma_a | Gamma_b |
|---|---|---|---|---|---|---|
| All | 171 | 2237.48 | 0.936 | 134.872 | 85.755 | 0.433 |
| Area | 68 | 1025.877 | 0.953 | 57.583 | 33.935 | 0.435 |
| Thickness | 68 | 191.599 | 0.938 | 53.641 | 34.049 | 0.434 |
| Subcortical | 35 | 132.63 | 0.913 | 20.977 | 17.484 | 0.435 |

*Rank-based inverse normal transformation*

It is important to carry out a rank-based inverse normal transformation of the measures, in order to have normally distributed z-scores as input for MOSTest. Without it, non-normally distributed measures can inflate p-values and thus elevate type-I error. Extended Data Figure 2 show the empirical distribution of MOSTest and min-P test statistics under the null (calculated via permutations), along with p-value calculated from the test, with the rank-based INT, showing correct behaviour. Figure 3 shows the distributions after running MOSTest without the transformation, leading to deviations, highlighting that this transformation is important for maintaining correct type-I error.

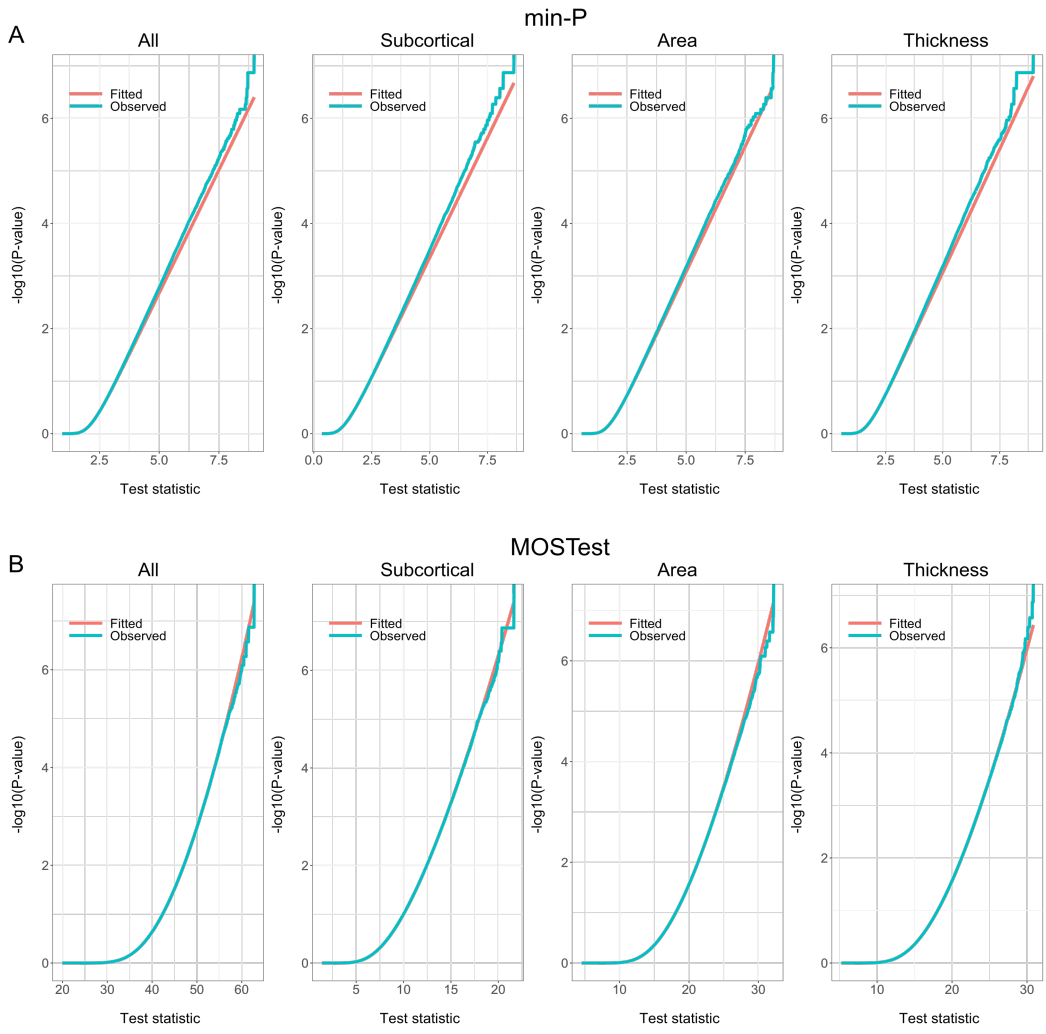


***Extended Data Figure 2.*** *Each subplot shows an empirical distribution of the min-P (top row) and MOSTest (bottom row) test statistics under null (calculated via permutations), along with p-value calculated from the test. Columns correspond to different sets of phenotypes included in the analysis. OX axis show the actual value of the test statistic: -log10(min-P), for the min-P test, and* $z' \mathbf{R}^{-1} z$ *for MOSTest. The "Observed" plot shows empirical distribution of the test statistic; "Fitted" plot shows p-values calculated from Gamma(a,b) distribution (MOSTest) and Beta(a,b) distribution (min-P) after fitting the two parameters to the observed data.*

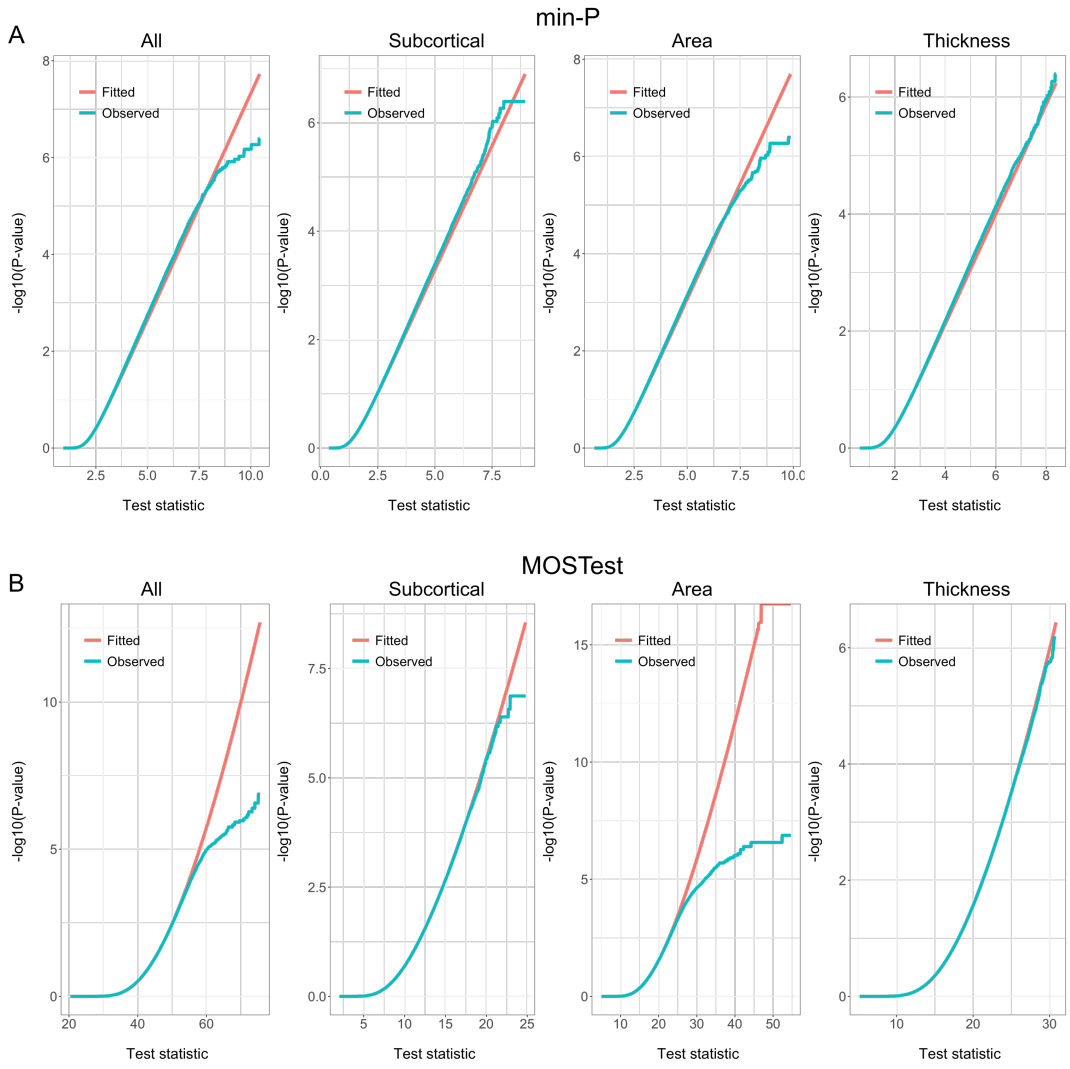


***Extended Data Figure 3.*** *Distribution of min-P and MOSTest p-values under permutation, without applying rank-based inverse normal transformation, showing large deflection in the tails of the distribution. Appearance as in the previous figure.*

*Simulations for validation of correct type-I error in the presence of polygenic signal*

We performed simulations on synthetic data to validate that MOSTest has correct type-I also in the presence of polygenic signal. We used the real genotype matrix of 26,502 individuals from our main analysis to simulate 171 phenotypes using simple additive genetic model $y = G\beta + \epsilon$, with the same phenotypic correlation as we observed in our combined set of feature (cortical area, cortical thickness and subcortical volumes). We randomly chose a set of 10K "causal" SNPs, but constrained them to odd chromosomes only, leaving even chromosomes free of genetic signal. 10K "causal" SNPs were shared across the 171 phenotypes, but each phenotype has its own randomly generated $\beta$ vector of genetic effects. SNP heritability of each phenotype was h2=0.3. Applying MOSTest to test data, we observe the resulting signal was completely flat for even chromosomes, showing that regions that are not in LD with causal variants aren't picked by MOSTest.

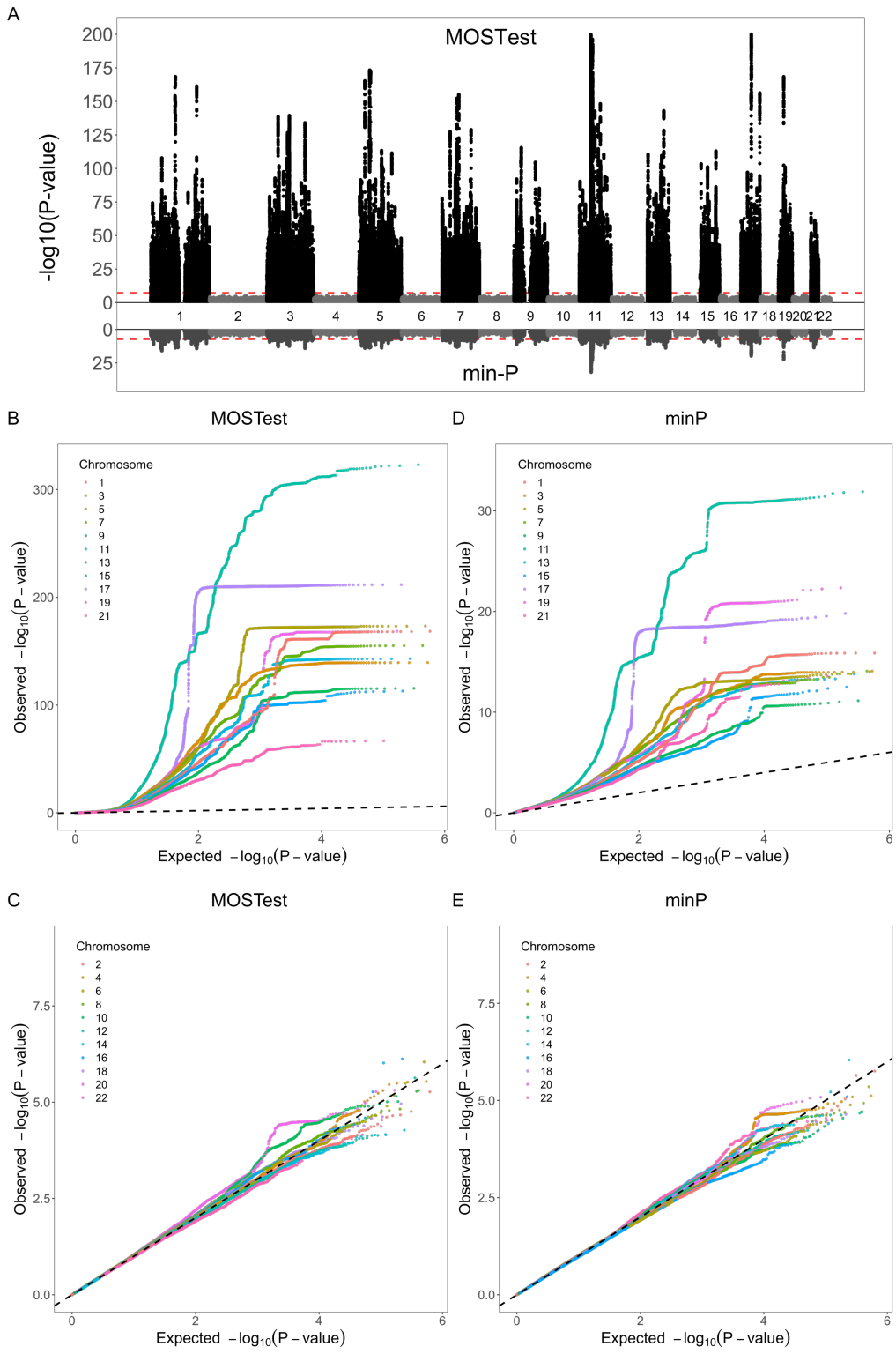


***Extended Data Figure 4****, showing Manhattan and per-chromosome QQ plots for a synthetic dataset of 175 simulated phenotypes, with h=0.3 heritability, with 10K causal variants randomly assigned to odd chromosomes. No signal is observed for even chromosomes (as expected).*

*Genomic inflation*

We applied LD score regression[27] to test for genomic inflation in MOSTest and min-P results. The results, listed in Extended Data Table 3, show no genomic inflation.

***Extended Data Table 3.*** *Genomic inflation analysis with LD Score Regression intercept (from partitioned LDSC 1kG phase3 reference), confirming no confounding effects (stratification, cryptic relatedness) in MOSTest p-values.*

| Feature set | Test | LambdaGC | Intercept from LDSC |
|---|---|---|---|
| All | min-P | 1.6524 | 0.9864 (0.0096) |
| All | MOSTest | 2.0217 | 0.9247 (0.015) |
| Subcortical | min-P | 1.5511 | 1.0062 (0.0086) |
| Subcortical | MOSTest | 1.7179 | 0.9742 (0.0106) |
| Area | min-P | 1.453 | 0.9913 (0.0093) |
| Area | MOSTest | 1.5733 | 0.9748 (0.0112) |
| Thickness | min-P | 1.4034 | 1.0085 (0.0068) |
| Thickness | MOSTest | 1.5254 | 0.9952 (0.0085) |

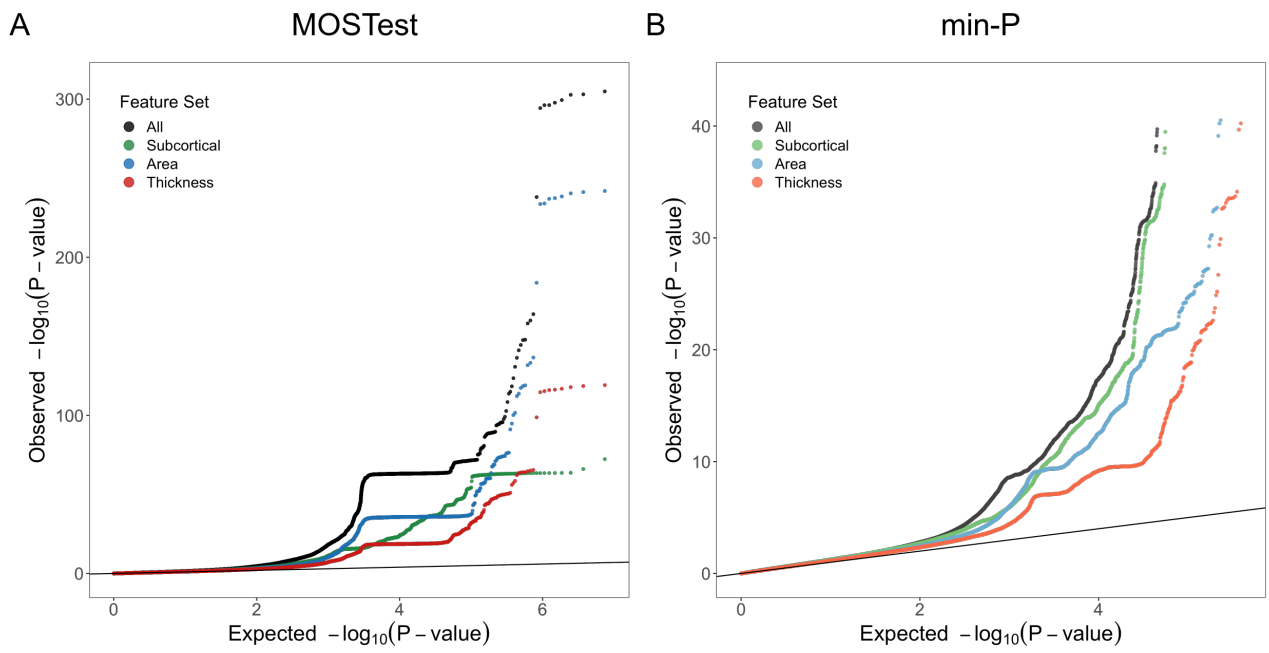


***Extended Data Figure 5.*** *Quantile-Quantile plots for the p-values derived from MOSTest (A) and min-P (B).*